JACS
JOURNAL OF THE AMERICAN CHEMICAL SOCIETY
Article
pubs.acs.org/JACS

Formation and Domain Partitioning of H-ras Peptide Nanoclusters: Effects of Peptide Concentration and Lipid Composition

Zhenlong Li,[†] Lorant Janosi,[†] and Alemayehu A Gorfe*

Department of Integrative Biology and Pharmacology, The University of Texas Health Science Center at Houston, 6431 Fannin St., Houston, Texas 77030, United States

Supporting Information

ABSTRACT: Experiments have shown that homologous Ras proteins containing different lipid modification, which is required for membrane binding, form nonoverlapping nanoclusters on the plasma membrane. However, the physical basis for clustering and lateral organization remains poorly understood. We have begun to tackle this issue using coarse-grained molecular dynamics simulations of the H-ras lipid anchor (tH), a triply lipid-modified heptapeptide embedded in a domain-forming mixed lipid bilayer [Janosi L. et al. *Proc. Natl. Acad. Sci. U.S.A.* **2012**, *109*, 8097]. Here we use the same simulation approach to investigate the effect of peptide concentration and bilayer composition on the clustering and lateral distribution of tH. We found no major difference in the clustering behavior of tH above a certain concentration. However, the simulations predict the existence of a critical concentration below which tH does not form nanoclusters. Moreover, our data demonstrate that cholesterol enhances the stability of tH nanoclusters but is not required for their formation. Finally, analyses of peptide distributions and partition free energies allowed us to quantitatively describe how clustering facilitates the accumulation of tH at the interface between ordered and disordered domains of the simulated bilayer systems. These thermodynamic insights represent some of the key elements for a comprehensive understanding of the molecular basis for the formation and stability of Ras signaling platforms.

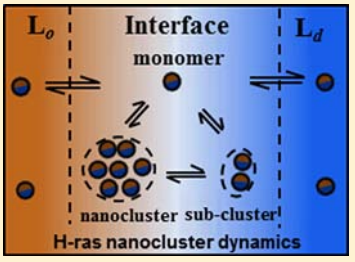

INTRODUCTION

Ras proteins are guanine triphosphate (GTP)-hydrolyzing enzymes that act as molecular switches to regulate cell proliferation, differentiation, and development.[1] H-, N-, and K-ras proteins are ubiquitously expressed in humans, and somatic mutations on these proteins are associated with ∼30% of all human cancers.[1] Ras proteins share a nearly identical catalytic machinery but differ in their C-terminal hypervariable (HVR) region, which contains a lipid-modified motif required for binding to specific membrane microdomains.[1,2] The minimal membrane-binding motif, also called the lipid anchor, of Ras proteins is well characterized.[3−5] The mechanism by which individual Ras lipid anchors attach to cellular or model membranes has also been investigated experimentally (for reviews see refs 6 and 7) and computationally.[8−14] As a result, the atomic interactions responsible for the insertion of Ras lipid anchors into fluid-phase phospholipid bilayers are relatively well established.[15−17] However, this knowledge alone is not sufficient to explain recent observations about the specific spatiotemporal organization of multiple Ras proteins on bilayer surfaces.[2,18,19]

To better understand the process of assembly and lateral organization of Ras proteins on membrane surfaces, numerous biophysical and cell biological experiments have been carried out on the full-length protein[3,4,20−22] as well as on simplified model peptides representing different Ras lipid anchors.[5,23−25] An emerging consensus is that different Ras lipid anchors have different preferences for raft-like liquid-ordered (L_o) and nonraft liquid-disordered (L_d) membrane domains.[2] Specifically, the farnesylated and dually palmitoylated lipid anchor of H-ras prefers cholesterol-enriched L_o domains;[18] the farnesylated and singly palmitoylated lipid anchor of N-ras predominantly localizes at the boundary between L_o and L_d domains;[26] and the farnesylated and polycationic lipid anchor of K-ras resides at disordered L_d domains.[22] The concept of chain packing[27−29] in phospholipid bilayers, which states that optimal packing occurs between lipids of the same chain length and saturation, offers an appealing institutive explanation for these observations. According to this theory, proteins (or peptides) modified by saturated palmitoyl lipids likely partition into L_o domains rich with saturated lipid species, whereas those modified by unsaturated and branched prenyl lipids likely partition into L_d domains enriched with unsaturated lipids. However, this does not readily predict the domain preference of proteins that are modified by multiple lipid types, such as N- and H-ras, because the balance of forces associated with different lipid modifications is hard to predict without a direct quantitative measure. Aiming at filling this gap, recent theoretical studies have begun to shed light on the thermodynamic basis for domain-specific partitioning of individual lipid-modified peptides and hybrid lipids.[29−37] For instance, Uline et al.[29] used a mean-field approach to calculate the L_o/L_d partition coefficients of several lipid chain anchors. They found that the chain length, degree of saturation, and architecture of the anchor as well as the composition of the

Received: August 3, 2012
Published: September 20, 2012

 © 2012 American Chemical Society dx.doi.org/10.1021/ja307716z | *J. Am. Chem. Soc.* 2012, 134, 17278−17285

membrane modulate the domain preference of the lipid anchors. Similar observations have been made in molecular dynamics (MD) simulations of hybrid lipids and the H-ras lipid anchor.[30,37] However, it is still unclear how lipid-modified peptides and proteins self-assemble and then laterally organize in membrane domains or how clustering and lateral segregation might be coupled. The present work focuses on this issue.

Coarse-grained molecular dynamics (CGMD) simulations, which allow sampling of phase space in larger length and time scale than is possible by fully atomistic models, have been successfully used to characterize the aggregation behavior of a variety of surface-bound and transmembrane proteins.[38−42] Recently, we have used this approach to study the clustering and lateral segregation behavior of the H-ras lipid anchor (tH) in a bilayer of coexisting L_o and L_d domains.[37] We found that 30−40% of the tH molecules form dynamic nanoclusters that exist in equilibrium with the nonclustered fraction. Similarly, both depalmitoylated and defarnesylated tH variants self-assemble into transient clusters of 4−10 molecules, but they exhibit dramatically different preferences for L_o and L_d domains. The current work provides insights into the interplay between clustering and domain partitioning based on new simulations in which concentrations of tH and cholesterol were systematically varied.

METHODS

Model Systems and Simulation Setup. The starting configuration for the current simulations is a previously reported[37] bilayer system composed of 960 dipalmitoylphosphatydilcholine (DPPC), 576 dilinoleaylphosphatydilcholine (DLiPC), and 384 (20%) cholesterol in which 64 tH peptides were inserted into the lower leaflet (system $S_{64,20}$). A detailed description of the models and protocols for system preparation, simulation setup, and other relevant information can be found in our recent report.[37] Here we briefly describe the setup of the simulations with variable tH and cholesterol content.

We carried out seven simulations using GROMACS 4.3.[43] The simulations involved a fully solvated mixed bilayer made up of DPPC and DLiPC lipids, plus a variable number of tH and cholesterol. DPPC, DLiPC, cholesterol, water, and ions were modeled by the MARTINI version 2.0 CG force field.[44,45] A MARTINI compatible CG model of tH was built as described previously[37] and in the Supporting Information (SI). Figure 1 shows both the atomic and CG representations of tH, a seven-residue peptide comprising Gly^{180}, Pa^{181}, Met^{182}, Ser^{183}, Pa^{184}, Lys^{185}, and Fa^{186} and a carboxymethylated C-terminus, where Pa and Fa represent Cys residues post-translationally modified by palmitoyl and farnesyl lipids, respectively.

To generate systems with 16, 32, and 48 tH molecules ($S_{16,20}$, $S_{32,20}$, and $S_{48,20}$) 48, 32, and 16 tHs were randomly deleted from $S_{64,20}$ along with the corresponding number of chloride ions to maintain total charge neutrality. Note that in this set of simulations the cholesterol content was kept fixed to the original value of 20%. In another set of simulations, the fraction of cholesterol in the bilayer was set to 0, 11, or 27% by removing or adding the appropriate number of cholesterol molecules from $S_{64,20}$. Specifically, all of the cholesterol molecules in $S_{64,20}$ were removed to generate system $S_{64,00}$, 192 cholesterols were removed in the case of $S_{64,11}$, and 192 cholesterols were added (equally distributed in each leaflet) to generate system $S_{64,27}$. It is worth mentioning that because increasing the cholesterol content from 0 to 27% expanded the simulation box area only by ∼3%, the number of peptides per unit area is comparable in all four of these systems. Each system was then energy minimized, equilibrated, and simulated for at least 40 μs at 28 °C and 1 atm. Table 1 summarizes the composition, the simulation length, and the potential of each system to form coexisting lipid domains. Note that all simulation times in Table 1 and the rest of this report are effective times, which is 4 times the real simulation time because the water diffusion coefficient in this CG model is around 4 times faster than in an atomistic model.[44]

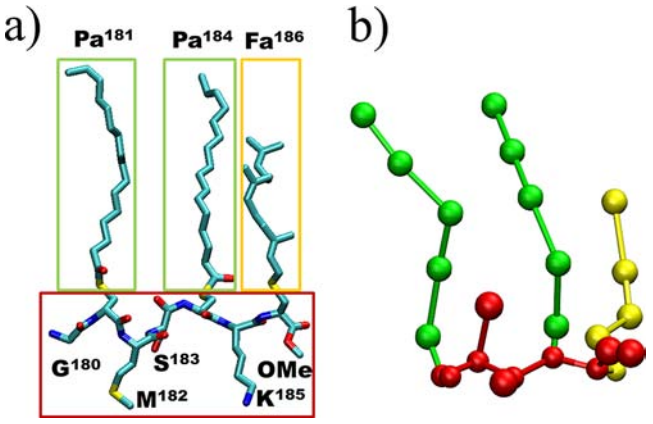

Figure 1. Structure of the tH peptide. The amino acid sequence of tH is labeled based on residue numbering in the full-length H-ras protein. (a) All atom representation with carbon in cyan, oxygen in red, nitrogen in blue, and sulfur in yellow. Hydrogen atoms are not shown. (b) A MARTINI-based CG representation of tH with Gly, Met, Ser, and Lys side chains as well as the peptide backbone shown in red, palmitoyl (Pa) in green, and farnesyl (Fa) in yellow, as shown by the correspondingly colored boxes in (a).

Analysis. Trajectories were analyzed using a combination of GROMACS tools and in-house tcl scripts in conjunction with VMD.[46] Analysis of the time evolution of the bilayer structural properties and tH clustering (discussed later) confirmed that full equilibration was achieved within 24 μs of each simulation. Therefore, the bilayer and the tH nanoclusters were analyzed based on the next 16 μs data (i. e., from 24 to 40 μs).

The composition and size of individual nanoclusters at equilibrium were monitored to characterize the dynamics of the nanoclusters. In this analysis, the molecular indices and cluster size of a nanocluster at a given time t', which represents the time point at which we begin to follow the cluster, were recorded and then monitored with time. The identity of a nanocluster at any time t remains unchanged until more than half of its constituent molecules have left. The evolution of cluster composition with time is monitored using a molecular expulsion autocorrelation function $f(t)$.[37,47] In this function, all tH molecules in a given cluster (a cluster is defined here as an aggregate of four or more peptides) of specific size were marked as "native" at t'. A "native" peptide is unmarked if it leaves the cluster either as a monomer or as part of another aggregate, and $f(t)$ was then calculated as

$$f(t) = \left\langle \frac{M(t') - M_{\text{leave}}(t)}{M(t')} \right\rangle \tag{1}$$

where $M(t')$ is the cluster size at t' and $M_{\text{leave}}(t)$ is the accumulating number of "native" peptides that are no longer part of the cluster at time t. The cluster size at t, $N(t)$, was also recorded to monitor the cluster size evolution with time.

Peptide density profiles at equilibrium were calculated by evenly dividing the simulation box into 88 bins of width ∼0.25 nm. For each bin, the time-averaged peptide density, ρ, was calculated as a function of position along the direction perpendicular to the domain boundary. The distribution profile of peptides in different domains was then calculated by normalizing the density profile, which was then used to estimate the probability of finding a peptide at a specific position on the bilayer surface. The free energy of partition of tH at the domain boundary (int) relative to the L_o and L_d domains, ΔG, was estimated as

$$\Delta G = -RT \ln\left(\frac{\rho_{\text{int}}}{\rho_{\text{b}}}\right) \tag{2}$$

where R is the gas constant, T is the temperature in Kelvin, and ρ_{int} and ρ_{b} are the average densities of tH at the boundary and the bulk

dx.doi.org/10.1021/ja307716z | J. Am. Chem. Soc. 2012, 134, 17278−17285

Table 1. Summary of the CGMD Simulations Analyzed in This Study*

$S_{a,b}$	N_p (tH/lipid)	N_c (%)	length [μs]	lipid domains	tH clusters	used for analysis [μs]
$S_{16,20}$	16 (0.008)	384 (20)	40	yes	no	16
$S_{32,20}$	32 (0.017)	384 (20)	48	yes	yes	16
$S_{48,20}$	48 (0.025)	384 (20)	40	yes	yes	16
$S_{64,20}$	64 (0.033)	384 (20)	40	yes	yes	16
$S_{64,00}$	64 (0.042)	0 (0)	80	no	yes	16
$S_{64,11}$	64 (0.037)	192 (11)	40	dynamic	yes	16
$S_{64,27}$	64 (0.030)	576 (27)	40	yes	yes	16

*$S_{a,b}$ represents the name of the system, where 'a' is the number of tH molecules and 'b' is the fraction of cholesterol in the bilayer. N_p is the number of tH molecules, while tH/lipid refers to peptide-to-lipid ratio. N_c is the number of cholesterol molecules in the system, with its percentage relative to the total number of lipids given in brackets. The number of DPPC lipids is 960, and that of DLiPC is 576 in all simulations. Each simulation was run for at least 40 μs, but only the equilibrated 24–40 μs data were used for analysis of equilibrium properties.

region of a domain, respectively. Equation 2 relies on the inversion of the probability density distribution profile (ρ) based on the relationship

$$G_p = -RT\ln\rho \tag{3}$$

where G_p is an intermediate variable. ΔG can then be readily calculated from the difference between the average G_p at the interface and in the bulk region of a domain. For the purpose of these calculations, ρ_{int} was calculated for a ~2 nm wide region centered at the peak of the tH density profile. The average density of peptides at the L_o domain, ρ_o, was calculated as the average density of a ~4 nm wide region in the middle of the L_o domain. The average density of peptides at the L_d domain, ρ_d, was calculated similarly after defining an L_d domain as the DLiPC-dominated region of size ~2 nm. The smaller size of the L_d domain reflects the lower percentage of DLiPC lipids in the simulations. Error bars for ΔG were estimated by propagating the standard deviation of G_p in different regions.

RESULTS AND DISCUSSION

We have shown recently that wild-type tH and its partially delipidated counterparts form clusters of comparable size.[37] Depending on the nature of the lipid modification, these clusters segregate to either the ordered or disordered lipid domains or the boundary between them. In the subsequent sections of this paper, we describe how clustering, dynamics, and lateral organization behaviors of the triply lipidated wild-type tH are modulated by peptide concentration and membrane environment relative to data from a $S_{64,20}$ system reported before.[37]

Lipid Domain Formation and tH Clustering. The time evolutions of the bilayer structural properties (Figure 2a), and the profile of tH cluster formation (Figure 2b), show that all of the simulations are well equilibrated. Moreover, two stable, striped lipid domains have formed in all but two of the simulations (Table 1). Since lipid demixing was limited in the 0% and 11% cholesterol systems (systems $S_{64,00}$ and $S_{64,11}$), no stable lipid domains were observed (Figure 3). To check if domain formation is limited by the length of of the simulations, $S_{32,20}$ and $S_{64,00}$ were extended to 48 and 80 μs, respectively. We found no major changes in the domain behavior of the bilayer or the clustering behavior of tH. The lack of striped domains in $S_{64,00}$ (Figure 3a) is consistent with the fact that cholesterol is required for phase separation at the current simulation temperature of 28 °C.[37] That the lipid domains were found to be small and unstable in the presence of 11% cholesterol (Figure 3b) suggests this cholesterol concentration is below the threshold needed for an extensive DPPC/DLiPC segregation. To our knowledge, the phase diagram for a DPPC/DLiPC/cholesterol mixture is not known. Judging from the corresponding phase diagram of a similar mixture containing dioleoylphosphatydilcholine instead of DLiPC,[48] we surmise that 11% cholesterol would be below the concentration range for a L_o/L_d domain coexistence. Therefore, our models accurately captured the expected domain behavior of our lipid mixtures under the simulation conditions used here.

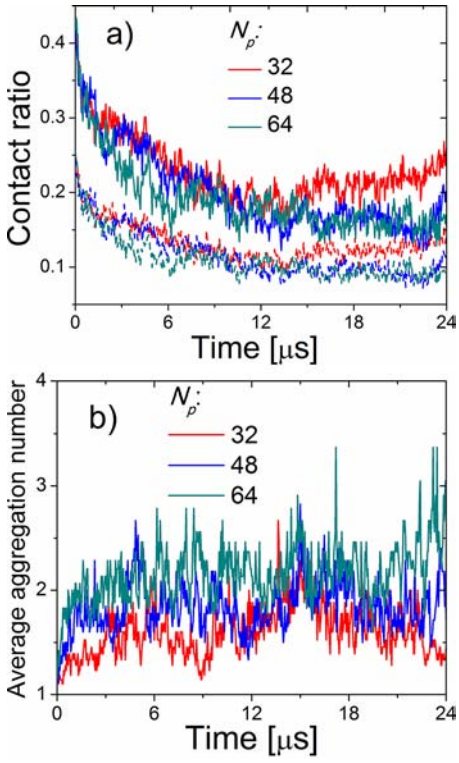

Figure 2. Time evolution of the bilayer structure and the average cluster size for systems containing different number of tH (N_p = 32, 48, 64). (a) Time evolution of the incompatible contact ratio between DPPC and DLiPC in the lower leaflet calculated as the fraction of DLiPC (dashed line) and DPPC (solid line) lipids that are within 7.5 Å of a central DPPC (DLiPC) molecule, respectively. (b) Time evolution of the number-averaged cluster size (N_n). Similar profiles were obtained for the rest of the simulations.

Consistent with our previous observation,[37] the presence of tH did not significantly affect the phase behavior of the bilayer, while analyses of aggregation numbers (Table 1, Figure 4) indicate that tH clustering has occurred in all but one ($S_{16,20}$) of the simulations. Clustering was always fast, being complete within the first 6 μs (Figure 2b) in all simulations with N_p = 32 or higher. However, no significant clustering took place in

dx.doi.org/10.1021/ja307716z | J. Am. Chem. Soc. 2012, 134, 17278–17285

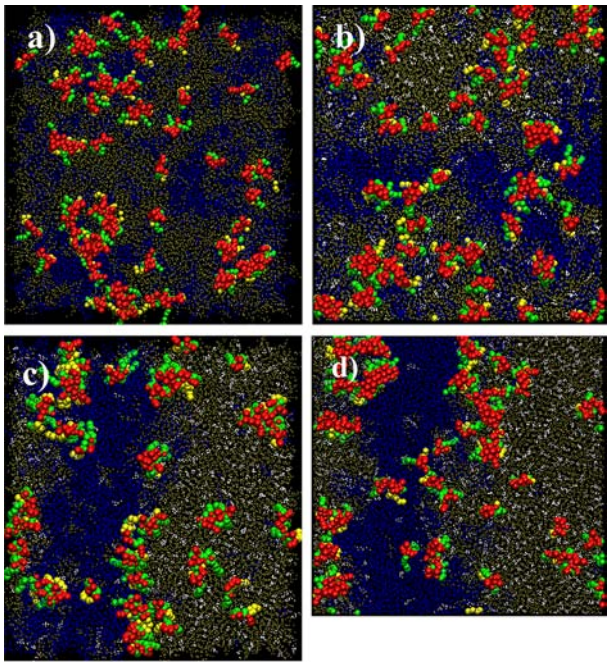

Figure 3. Simulation snapshots at t = 24 μs for systems with different cholesterol content. (a) $S_{64,00}$, no cholesterol; (b) $S_{64,11}$, 192 cholesterol (11%); (c) $S_{64,20}$, 384 cholesterol (20%); and (d) $S_{64,27}$, 576 cholesterol (27%). Color codes: DPPC in tan, DLiPC in blue, cholesterol in white, peptide backbone and nonlipidated side chains in red, and palmitoyl and farnesyl in green and yellow, respectively. All snapshots were rendered by VMD.[46]

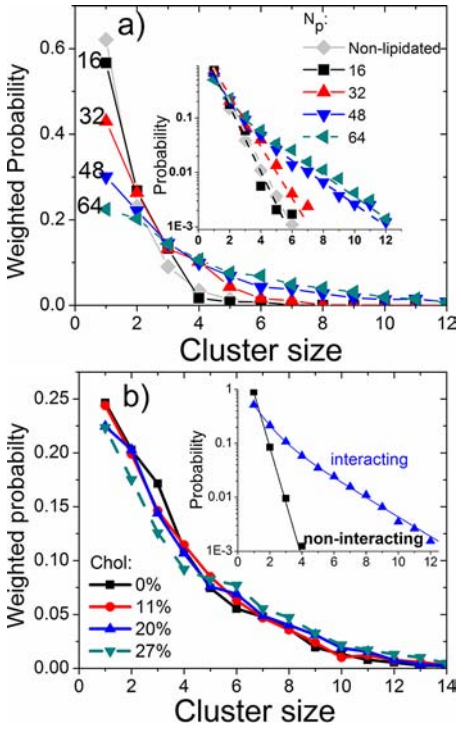

Figure 4. tH cluster size distributions from simulations at various concentrations of tH and cholesterol. (a) Weighted cluster size probability distribution of systems containing 16 (black), 32 (red), 48 (blue), and 64 (cyan) tH peptides derived from simulations $S_{16,20}$, $S_{32,20}$, $S_{48,20}$, and $S_{64,20}$, respectively. The gray dashed line represents the distribution for 64 tH peptides that lack Pa and Fa (with all tH lipid tails replaced by the parent Cys). Inset: the nonweighted cluster size distribution in a semi-logarithmic scale. (b) Weighted cluster size distribution of 64 tH molecules on a bilayer whose cholesterol content was 0% (black), 11% (red), 20% (cyan), and 27% (blue) obtained from simulations $S_{64,00}$, $S_{64,11}$, $S_{64,20}$, and $S_{64,27}$, respectively. Inset: The nonweighted cluster size distribution for the system with 27% cholesterol (one of the "interacting" systems) fitted with a double-exponential decay function (blue) and for a noninteracting system derived from a numerical simulation of 64 inert particles fitted with a single exponential decay function. Except for the inset of panel (b), lines are for eye guide only.

system $S_{16,20}$ within the time scale of the simulation. The following section focuses on the physical basis for this observation and its implication for future experiments. We will then turn to the role of cholesterol on tH clustering.

Effect of Protein Concentration on the Formation and Dynamics of tH Nanoclusters. *Cluster Size.* Figure 4a displays the distribution of tH monomers and aggregates of various sizes derived from simulations in which the number of peptides (N_p) was 16, 32, 48, and 64 with a fixed cholesterol content of 20%. One can readily see that most of the profiles are similar, but there are some crucial differences that warrant a closer look. First, the tH cluster distribution in $S_{16,20}$ is almost exactly identical to that of a peptide without lipid modification (where each of the palmitoyls and farnesyl were mutated to the parent cysteine, gray in Figure 4a). Both of these distributions, in turn, are almost identical to the distribution of an idealized noninteracting particle system with complete spatial randomness.[37] On average, 9 out of 16 tHs in $S_{16,20}$ remain monomer while the other 7 form dimers or trimers. Defining nanoclusters as aggregates of four or more tH molecules,[37] we conclude that tH does not form nanoclusters at this concentration within the time scale of the simulations.

Second, whereas the number of tH in clusters of size four or larger (the clustered fraction) is zero in $S_{16,20}$, increasing N_p by 2-, 3-, or 4-fold (systems $S_{32,20}$, $S_{48,20}$ and $S_{64,20}$) increases the clustered fraction to 14, 28, and 34%, respectively (Figure 4a). The corresponding total numbers of monomers, dimers, and trimers (i. e., the nonclustered fraction) decrease by similar magnitudes. Notice that the clustered fraction in systems $S_{48,20}$ and $S_{64,20}$ is not significantly different and roughly falls within the 30−40% range estimated from cell-based experiments.[18] The absence of nanoclusters at N_p = 16, coupled with the doubling of the clustered fraction between N_p = 32 and 48 and the smaller increase when N_p is further increased to 64, suggests the existence of two critical concentrations: (i) a minimum, below which nanoclustering does not occur, and (ii) a maximum, at which tH nanoclustering reaches an eventual saturation.

Dynamics and Internal Interaction. In addition to the aforementioned effect of peptide concentration on the formation of nanoclusters, there are variations in the dynamics and internal interaction of the tH aggregates derived from the four simulations. Illustrating this point, the inset in Figure 4a shows that the cluster size distribution in $S_{16,20}$ can be fitted to a single-exponential function, as are the distributions of the nonlipidated and noninteracting particle systems. In contrast, the distribution exhibits a double-exponential decay for the two systems with the highest tH concentration ($S_{48,20}$ and $S_{64,20}$). The distribution in $S_{32,20}$ is somewhat different and lies between these two extremes. The single exponential decay indicates the lack of strong interaction within small aggregates, which appear to be formed via random collision. In the case of the biphasic distribution, the first phase suggests sharp differences between

dx.doi.org/10.1021/ja307716z | J. Am. Chem. Soc. 2012, 134, 17278−17285

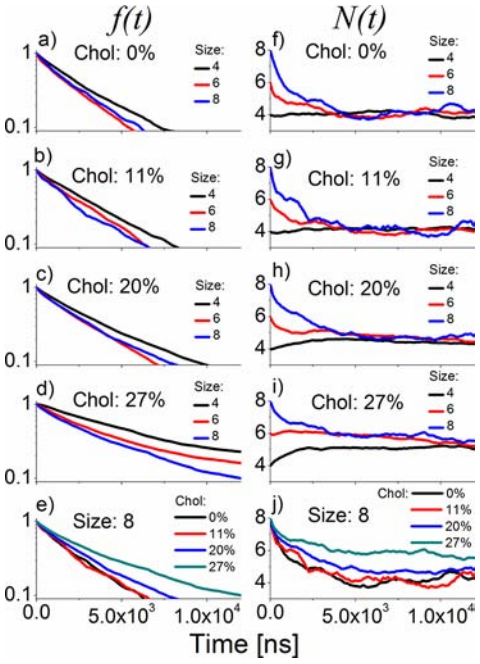

Figure 5. Nanocluster dynamics for systems with different cholesterol content. The first column (a–e) is the molecular expulsion ACF ($f(t)$), and the second column (f–j) is the time evolution of the size of individual clusters ($N(t)$). The first four figures in each column represent the $f(t)$ and $N(t)$ for systems with 0% (a,f), 11% (b,g), 20% (c,h), 27% (d,i) cholesterol and initial cluster size of 4 (black), 6 (red) and 8 (blue). Panels e and j show $f(t)$ and $N(t)$ of clusters with initial size 8 for systems with 0% (black), 11% (red), 20% (cyan), 27% (blue) cholesterol.

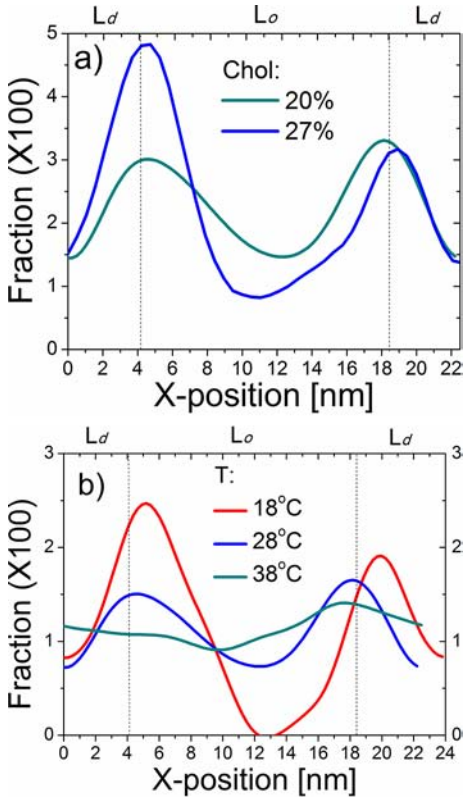

Figure 6. tH distribution profiles in membrane domains. (a) The probability distribution of tH along the x dimension of the simulation box (i.e., perpendicular to the interdomain line) from $S_{64,20}$ (blue) and $S_{64,27}$ (green) simulated at 28 °C. (b) Same as in (a) but for a 64 tH system containing 20% cholesterol simulated at 18, 28, and 38 °C. Dashed lines indicate the approximate center of the domain boundary derived from bilayer composition analysis.

the average number of monomers, dimers, and trimers, whereas the slow second phase suggests a similar average number of larger clusters. The biphasic distribution is also related to the generally more dynamic nature of small aggregates than nanoclusters and to the fact that dimers and trimers are held together by weak nonspecific interactions, while cumulative interactions in large clusters produce tighter packing. This is consistent with our previous observation that tH within clusters adopts a specific conformation and organizes in a manner that allows for maximum inter-tH and tH–lipid interactions.[37]

Predicting a Critical Cluster Concentration for tH. A number of important lessons can be drawn from the data described above. In the absence of lipid modification, the peptides partition to solvent where nanoclusters cannot form. In contrast, even at a relatively low concentration (e.g., N_p = 32), a fraction of the lipid-modified membrane-bound tH quickly assembles into clusters. This can be explained, in part, by the reduced dimensionality in the 2D surface of the bilayer and therefore the lower entropic cost of association. The extra degree of freedom in the 3D environment of the bulk solvent favors monomers or small aggregates even at a high tH concentration of N_p = 64. Thus, tH nanoclustering is not a random event facilitated by high concentration but rather a consequence of lipid modification and hence membrane binding.

However, in the same manner as many surfactants do not form micelles below a certain critical concentration,[49] the amphipathic tH does not form nanoclusters below a "critical cluster concentration" (ccc). Unfortunately, the published cell-based experiments[18] do not provide any clear indication as to what tH's ccc might be. This is perhaps related to the difficulty of systematically varying the peptide-to-lipid ratio (p/l) in cell membranes, which is required to monitor clustering as a function of peptide concentration. Our simulations predict that a p/l ≈ 0.01 may represent the ccc for tH. This value is roughly between 0.008 in $S_{16,20}$ where no clustering was observed and 0.017 in $S_{32,20}$ where partial clustering has occurred. The amount of the clustered fraction changes little at p/l values of 0.03 or higher, such as in systems $S_{48,20}$ and $S_{64,20}$. Though this appears to be in qualitative agreement with the experimentally observed fixed clustered fraction at different expression levels of Ras,[18] it is not conclusive because extrinsic factors in cells, such as the actin cytoskeleton and integral membrane proteins, are also likely to play a role.[18] Therefore, verification of our prediction awaits a suitable experimental technique in an *in vitro* setting.

Role of Cholesterol in tH Clustering and Dynamics. *Cholesterol is Required for the Formation of Striped Lipid Domains.* To evaluate the influence of lipid domain stability on tH clustering, we carried out three additional simulations in which the peptide concentration was fixed to N_p = 64, while the cholesterol content of the bilayer was set to 0, 11, and 27% (simulations $S_{64,00}$, $S_{64,11}$, and $S_{64,27}$). We reiterate that these simulations were conducted to study the effect of lipid phase behavior on tH clustering as cholesterol is known to facilitate phase separation and stabilize membrane domains. Thus, as mentioned above, systems $S_{64,00}$ and $S_{64,11}$ were not expected to result in phase separation, whereas $S_{64,27}$ should lead to more

dx.doi.org/10.1021/ja307716z | J. Am. Chem. Soc. 2012, 134, 17278–17285

Table 2. Estimation of the Partition Free Energy (in kJ/mol) of tH at the Interface Relative to the L_d and L_o Domains[a]

N_p	16			32			48			64		
$<s_w>$	1	2.4	–	1	2.3	4.6	1	2.4	5.3	1	2.4	6.6
$\Delta G_{int/L_d}$	−2.0 (0.4)	−4.5 (1.0)	–	−2.2 (0.3)	−3.7 (0.2)	−4.2 (0.6)	−1.0 (0.1)	−2.4 (0.1)	−1.6 (0.6)	−1.0 (0.1)	−1.8 (0.1)	−2.7 (0.3)
$\Delta G_{int/L_o}$	−1.8 (0.4)	−5.1 (1.1)	–	−0.9 (0.2)	−2.7 (0.2)	−5.3 (0.2)	−0.7 (0.1)	−1.8 (0.1)	−3.3 (0.6)	−0.5 (0.1)	−0.9 (0.1)	−5.5 (0.3)

[a] $<s_w>$ is the weighted average cluster size for monomer, dimer/trimer, and large clusters. $\Delta G_{int/L_d}$ is the partition free energy between the interface and the L_d domain, and $\Delta G_{int/L_o}$ is the corresponding partition free energy between the interface and the L_o domain. Standared errors are indicated in brackets.

stable lipid domains than the reference system $S_{64,20}$. This means that L_o/L_d domains were expected to coexist only in $S_{64,20}$ and $S_{64,27}$. Consistent with these expectations, extensive lipid segregation occurred in $S_{64,20}$ and $S_{64,27}$, while no striped domains were observed in systems $S_{64,00}$ and $S_{64,11}$ (Figure 3).

Cluster Size and Dynamics. The cluster size distributions are similar in all four of these simulations, except for a slight increase in the fraction of large clusters at high cholesterol content (Figure 4b). Clearly, tH clustering exhibits negligible dependence on the cholesterol content of the bilayer. At first glance, this finding appears to contradict earlier cell-based experiments that suggested cholesterol dependence of tH clustering.[18] In order to resolve this apparent contradiction, we looked at the dynamics of the nanoclusters in each system based on the time-dependent autocorrelation function (ACF) of molecular expulsion $f(t)$ (Figure 5, first column) and the time evolution of individual clusters $N(t)$ (Figure 5, second column) (see Methods section). The molecular expulsion ACF $f(t)$ reflects how quickly a nanocluster loses its "native" components by either single molecule or subcluster expulsion. In contrast, the size evolution of an individual cluster, $N(t)$, tells us how the size of an existing cluster changes with time through the joint effect of molecular expulsion and addition. Since the clusters in all systems are polydisperse in size, i.e., contain clusters of different size (Figure 4), we calculated these quantities for three representative cluster sizes: 4, 6, and 8. As shown in the first four plots of each column in Figure 5, both $f(t)$ and $N(t)$ are always dependent on the initial cluster size. Within the same system, large clusters (size 6 and 8) lose their "native" components more quickly than small clusters (size 4) (Figure 5a–d). In addition, the size of large clusters always drops quickly to the optimal cluster size (which is reflected by the convergence of $N(t)$ to a single value from different initial sizes) (Figure 5f–i). This trend indicates that declustering forces originating from the thermodynamic fluctuation and conformational entropic penalty prevent nanoclusters from growing indefinitely. By comparing clusters of the same size derived from simulations with different cholesterol content (Figure 5e,j, also see Supporting Information), we found that the larger the cholesterol content, the slower the rate at which the cluster loses its "native" components. Furthermore, the optimal cluster size increases with increasing cholesterol content (Figure 5e,j).

Overall, the larger the cholesterol content the more stable is the cluster in terms of both composition and size, consistent with the fact that cholesterol enhances lipid packing and reduces bilayer fluidity.[50,51] Moreover, for the two systems with the largest cholesterol content, the formation of lipid domains increases the effective concentration of tH at the domain boundaries and thereby drives the dynamic equilibrium toward clustering. This relationship between lipid domain stability and cluster dynamics is in agreement with the temperature dependence of tH clustering, where we have shown that nanocluster stability increases with decreasing temperature and hence increasing domain stability.[37] It follows that clustering is an intrinsic property of lipidated Ras peptides that does not require cholesterol, but cholesterol facilitates lipid phase separation and thereby increases nanocluster stability.

Implication for Ras Signaling. It is tempting to speculate that the reported[18] absence of tH nanoclusters in cholesterol depleted cell membranes might be a consequence of the limited time resolution of the spectroscopic techniques rather than tH declustering. We predict that future experiments with

submicrosecond or better resolution might capture fast-exchanging nanoclusters in mixed bilayers lacking cholesterol or even in pure bilayers that do not form microdomains. From a functional perspective, it stands to reason that the potential to form nanoclusters under various membrane environments is encoded in the sequence and structure of Ras proteins. However, the clusters have to be stabilized by lipid domains to remain intact long enough for signaling events to occur. In this manner, cells can regulate the lateral organization of Ras and its interaction partners by reconfiguring the local composition of the bilayer, possibly in an energy-dependent manner.

Insights into the Lateral Organization and Domain Partitioning of tH Nanoclusters. Comparison of the wild-type tH with its depalmitoylated and defarnesylated counterparts demonstrated that the palmitoyl tails tend to pull the peptide toward the L_o domain, while farnesyl drives it toward the L_d domain.[37] This antagonistic action of the two lipid moieties leads to the accumulation of tH nanoclusters at the boundary between the L_o and L_d domains (see Figure 3b,c in ref 37). Similar observations have been made by others for hybrid lipids with one saturated tail and one unsaturated tail.[30,33−36] This holds true for each of the current simulations where stable L_o/L_d domains are formed. As an example, Figure 6a shows the distribution of tH across the bilayer (and perpendicular to the line of the domain boundary) for simulations $S_{64,20}$ and $S_{64,27}$. It is clear that tH accumulates in the region between the L_o and L_d domains, and preference for the domain boundary is highest for the system with the largest cholesterol content. Since cholesterol stabilizes the L_o domain, this data demonstrate once again that tH's preference for the domain boundary increases with increasing lipid domain stability.

To further examine this issue, we compared the tH distribution profiles in $S_{64,20}$, which was carried out at 28 °C, with two other previously reported[37] simulations performed at 18 and 38 °C (Figure 6b). The preference for the domain boundary is much higher at 18 °C where the lipid domains are most stable. There is negligible preference for any region of the bilayer at 38 °C where no clearly defined striped domain exists. This provides another example to the fact that tH preference for the domain boundary is a function of lipid segregation and domain stability. The data in Figure 6 also show that tH is more efficiently excluded from the L_o domain in simulations where lipid packing was enhanced by the effect of high cholesterol concentration or low temperature. Therefore, despite its two saturated lipid tails, tH is less compatible with the tightly packed DPPC lipids in the L_o domain than with the more flexible DLiPC lipids in the L_d domain. We conclude that tH lateral segregation is primarily a function of packing deficiency and that the same fundamental forces that underlie clustering also dictate lateral organization.[52]

Finally, in an initial effort to evaluate the affinity of tH for the domain boundary, we estimated the free energy of tH partitioning from the L_o and L_d domains to the interface (see Methods section). Oligomerization has been shown to amplify the partitioning preference of lipidated proteins to specific membrane domains,[53] consistent with the high concentration of nanoclusters of tH and its variants in different lipid domains,[37] and the additive effect of chain anchors on partition coefficient.[29] It is therefore interesting to evaluate the cluster size dependence of $\Delta G_{int/L_o}$ and $\Delta G_{int/L_d}$, assuming an uncorrelated partitioning behavior for tH aggregates of different size. Table 2 lists the weighted average aggregation number ($<s_w>$) grouped into monomers, dimers/trimers, and larger aggregates along with the corresponding values of $\Delta G_{int/L_o}$ and $\Delta G_{int/L_d}$. The result indicates that partitioning to the interface is energetically favored at all tH concentrations and cluster sizes and re-emphasizes the preference of tH for the interface and the enhancement of this preference by cluster growth.

■ CONCLUSIONS

In this work, we have examined the effect of peptide concentration and membrane composition on the clustering and domain preference of the H-ras lipid anchor (tH) using a coarse-grained molecular dynamics simulation approach. We have shown that tH molecules self-assemble into nanoclusters (with at least four molecules in each cluster) only above a certain threshold peptide concentration, which we call "critical cluster concentration" or "ccc". We have estimated the ccc for tH to be approximately 1 peptide per 100 lipids at 28 °C. Above this ccc, the fraction of tH in clusters was found to stabilize at around 30%. Moreover, as the concentration of tH increases, the cluster size distribution changes from a single-exponential decay to a double-exponential one, indicating that the driving force for clustering is relatively weak and that nanoclusters are dynamic in nature. We have also shown that tH cluster size distribution is only slightly dependent on cholesterol, but cholesterol increases the stability of the nanoclusters. Furthermore, in all of our simulations where lipid domains coexist, tH and especially large clusters of tH localize predominantly at the domain boundary.

More broadly, our simulations revealed the crucial role of the C-terminus of Ras proteins and membrane environment for nanocluster formation and provided detailed insights into the conditions required for Ras nanocluster formation. Our data also demonstrated the reversible nature of Ras nanoclustering and the coupling between Ras clustering and partitioning in membrane domains. These results therefore compliment the available macroscale experimental data by providing molecular insights and a thermodynamic foundation for the lateral organization of Ras on the plasma membrane and highlight the power of simulations to provide information that is extremely difficult to obtain by current experimental techniques. This information is crucial for a better understanding of Ras signaling platforms, which are potential targets to inhibit abnormal Ras signaling in cancer.

■ ASSOCIATED CONTENT

Supporting Information

CG model of tH and nanocluster dynamics are available. This information is available free of charge via the Internet at http://pubs.acs.org.

■ AUTHOR INFORMATION

Corresponding Author

Alemayehu.G.Abebe@uth.tmc.edu

Author Contributions

†These authors contributed equally.

Notes

The authors declare no competing financial interest.

■ ACKNOWLEDGMENTS

This work was supported in part by the National Institutes of Health (grant no.: 1R01GM10078). We thank the Texas Advanced Computing Center for computational resources and members of the Gorfe laboratory for fruitful discussions.

■ REFERENCES

(1) Karnoub, A. E.; Weinberg, R. A. *Nat. Rev. Mol. Cell Biol.* **2008**, *9*, 517.
(2) Abankwa, D.; Gorfe, A. A.; Hancock, J. F. *Semin. Cell Dev. Biol.* **2007**, *18*, 599.
(3) Rotblat, B.; Prior, I. A.; Muncke, C.; Parton, R. G.; Kloog, Y.; Henis, Y. I.; Hancock, J. F. *Mol. Cell. Biol.* **2004**, *24*, 6799.
(4) Abankwa, D.; Gorfe, A. A.; Inder, K.; Hancock, J. F. *Proc. Natl. Acad. Sci. U.S.A.* **2010**, *107*, 1130.
(5) Wang, T. Y.; Leventis, R.; Silvius, J. R. *Biochemistry* **2001**, *30*, 13031.
(6) Brunsveld, L.; Waldmann, H.; Huster, D. *Biochim. Biophys. Acta* **2009**, *1788*, 273.
(7) Gorfe, A. A. *Curr. Med. Chem.* **2010**, *17*, 1.
(8) Vogel, A.; Reuther, G.; Roark, M. B.; Tan, K. T.; Waldmann, H.; Feller, S. E.; Huster, D. *Biochim. Biophys. Acta* **2010**, *1798*, 275.
(9) Vogel, A.; Tan, K. T.; Waldmann, H.; Feller, S. E.; Brown, M. F.; Huster, D. *Biophys. J.* **2007**, *93*, 2697.
(10) Gorfe, A. A.; Pellarin, R.; Caflisch, A. *J. Am. Chem. Soc.* **2004**, *126*, 15277.
(11) Gorfe, A. A.; Babakhani, A.; McCammon, J. A. *Angew. Chem., Int. Ed. Engl.* **2007**, *46*, 8234.
(12) Gorfe, A. A.; Babakhani, A.; McCammon, J. A. *J. Am. Chem. Soc.* **2007**, *129*, 12280.
(13) Gorfe, A. A.; Hanzal-Bayer, M.; Abankwa, D.; Hancock, J. F.; McCammon, J. A. *J. Med. Chem.* **2007**, *50*, 674.
(14) Jensen, M. O.; Mouritsen, O. G.; Peters, G. H. *Biophys. J.* **2004**, *86*, 3556.
(15) Gorfe, A. A.; McCammon, J. A. *J. Am. Chem. Soc.* **2008**, *130*, 12624.
(16) Abankwa, D.; Gorfe, A. A.; Hancock, J. F. *Cell Cycle* **2008**, *7*, 2667.
(17) Gorfe, A. A.; Baron, R.; McCammon, J. A. *Biophys. J.* **2008**, *95*, 3269.
(18) Plowman, S. J.; Muncke, C.; Parton, R. G.; Hancock, J. F. *Proc. Natl. Acad. Sci. U.S.A.* **2005**, *102*, 15500.
(19) Hancock, J. F. *Nat. Rev. Mol. Cell Biol.* **2006**, *7*, 456.
(20) Prior, I. A.; Muncke, C.; Parton, R. G.; Hancock, J. F. *J. Cell Biol.* **2003**, *160*, 165.
(21) Weise, K.; Triola, G.; Janosch, S.; Waldmann, H.; Winter, R. *Biochim. Biophys. Acta* **2010**, *1798*, 1409.
(22) Weise, K.; Kapoor, S.; Denter, C.; Nikolaus, J.; Opitz, N.; Koch, S.; Triola, G.; Herrmann, A.; Waldmann, H.; Winter, R. *J. Am. Chem. Soc.* **2011**, *133*, 880.
(23) Huster, D.; Vogel, A.; Katzka, C.; Scheidt, H. A.; Binder, H.; Dante, S.; Gutberlet, T.; Zschörnig, O.; Waldmann, H.; Arnold, K. *J. Am. Chem. Soc.* **2003**, *125*, 4070.
(24) Vogel, A.; Reuther, G.; Weise, K.; Triola, G.; Nikolaus, J.; Tan, K. T.; Nowak, C.; Herrmann, A.; Waldmann, H.; Winter, R. *Angew. Chem., Int. Ed. Engl.* **2009**, *48*, 8784.
(25) Abankwa, D.; Hanzal-Bayer, M.; Ariotti, N.; Plowman, S. J.; Gorfe, A. A.; Parton, R. G.; McCammon, J. A.; Hancock, J. F. *EMBO J.* **2008**, *27*, 727.
(26) Nicolini, C.; Baranski, J.; Schlummer, S.; Palomo, J.; Lumbierres-Burgues, M.; Kahms, M.; Kuhlmann, J.; Sanchez, S.; Gratton, E.; Waldmann, H.; Winter, R. *J. Am. Chem. Soc.* **2006**, *128*, 192.
(27) Elliott, R.; Szleifer, I.; Schick, M. *Phys. Rev. Lett.* **2006**, *96*, 98101.
(28) Garbès Putzel, G.; Schick, M. *Biophys. J.* **2008**, *95*, 4756.
(29) Uline, M. J.; Longo, G. S.; Schick, M.; Szleifer, I. *Biophys. J.* **2010**, *98*, 1883.
(30) Schäfer, L. V.; Marrink, S. J. *Biophys. J.* **2010**, *99*, L91.
(31) Schäfer, L. V.; de Jong, D. H.; Holt, A.; Rzepiela, A. J.; de Vries, A. H.; Poolman, B.; Killian, J. A.; Marrink, S. J. *Proc. Natl. Acad. Sci. U.S.A.* **2011**, *108*, 1343.
(32) de Jong, D. H.; Lopez, C.; Marrink, S. J. *Farad. Discuss.* **2012**, in press.
(33) Brewster, R.; Pincus, P.; Safran, S. *Biophys. J.* **2009**, *97*, 1087.
(34) Brewster, R.; Safran, S. A. *Biophys. J.* **2010**, *98*, L21.
(35) Yamamoto, T.; Brewster, R.; Safran, S. *Europhys. Lett.* **2010**, *91*, 28002.
(36) Yamamoto, T.; Safran, S. A. *Soft Matter* **2011**, *7*, 7021.
(37) Janosi, L.; Li, Z.; Hancock, J. F.; Gorfe, A. A. *Proc. Natl. Acad. Sci. U.S.A.* **2012**, *109*, 8097.
(38) Parton, D. L.; Klingelhoefer, J. W.; Sansom, M. S. P. *Biophys. J.* **2011**, *101*, 691.
(39) Periole, X.; Huber, T.; Marrink, S. J.; Sakmar, T. P. *J. Am. Chem. Soc.* **2007**, *129*, 10126.
(40) Prakash, A.; Janosi, L.; Doxastakis, M. *Biophys. J.* **2010**, *99*, 3657.
(41) Janosi, L.; Prakash, A.; Doxastakis, M. *Biophys. J.* **2010**, *99*, 284.
(42) Domanski, J.; Marrink, S. J.; Schafer, L. V. *Biochim. Biophys. Acta* **2012**, *1818*, 984.
(43) Hess, B.; Kutzner, C.; van der Spoel, D.; Lindahl, E. *J. Chem. Theory Comput.* **2008**, *4*, 435.
(44) Marrink, S. J.; Risselada, H. J.; Yefimov, S.; Tieleman, D. P.; de Vries, A. H. *J. Phys. Chem. B* **2007**, *111*, 7812.
(45) Monticelli, L.; Kandasamy, S. K.; Periole, X.; Larson, R. G.; Tieleman, D. P.; Marrink, S. J. *J. Chem. Theory Comput.* **2008**, *4*, 819.
(46) Humphrey, W.; Dalke, A.; Schulten, K. *J. Mol. Graphics* **1996**, *14*, 33.
(47) Li, Z.; Dormidontova, E. E. *Soft Matter* **2011**, *7*, 4179.
(48) Davis, J. H.; Clair, J. J.; Juhasz, J. *Biophys. J.* **2009**, *96*, 521.
(49) Rosen, M. J. *Surfactants and Interfacial Phenomena, fourth edition*, John Wiley & Son Inc: Hoboken, NJ, 2012.
(50) Mitchell, D. C.; Litman, B. J. *Biophys. J.* **1998**, *75*, 896.
(51) Hofsäß, C.; Lindahl, E.; Edholm, O. *Biophys. J.* **2003**, *84*, 2192.
(52) Li, Z.; Gorfe, A. A. *Small GTPases* **2012**, *3*, 1.
(53) Levental, I.; Lingwood, D.; Grzybek, M.; Coskun, Ü.; Simons, K. *Proc. Natl. Acad. Sci. U.S.A.* **2010**, *107*, 22050.